

# Twisted electron impact elastic cross sections of polyatomic molecules: All active electron multicentered approach

Raul Sheldon Pinto\* and Rakesh Choubisa

Department of Physics, Birla Institute of Technology and Science, Pilani, Pilani Campus 333-031 (India)

(\*rchoubisa@pilani.bits-pilani.ac.in)

(Dated: September 17, 2024)

The methodology and computation of absolute elastic differential and integral (total) cross-sections of polyatomic molecules by twisted electron beam (Bessel Beam) impact is presented with  $CO_2$  as an example. The target molecule is modeled using multicentered wavefunctions with the correlation consistent quadruple zeta basis set cc-pVQZ and optimized by the post-Hartree Fock Coupled Cluster CCSD method. The electron density is obtained as a function of spatial coordinates and is used to calculate the elastic form factor while considering the active role of all electrons in the molecule. Coulomb direct potentials are used for the interactions of the incident beam with all electrons and nuclei in the First Born Approximation. Orientation averaging of the differential cross-section is performed to mimic experimental situations. The cross sections are calculated at intermediate energies ranging from 300eV to 1keV. The proposed methodology could be applied to any polyatomic molecule. The interactions of Bessel beams (Twisted Electron Beam) with topological charges  $m_l = 1, 2$ , and 3 are analyzed. The average over-impact parameters of the differential cross-sections representing the beam's interaction with a large number of uniformly transversely distributed molecules are also studied and presented. Finally, the molecules' Integral elastic cross-section (ICS) by plane waves and twisted beams is calculated and presented.

## I. INTRODUCTION

Elastic scattering of electrons is a phenomenon where an incident electron beam is scattered by a target without changing its kinetic energy and the magnitude of its momentum while changing only its direction. The quantum mechanical investigation of such phenomena involves computing cross sections, the quantities of interest that reveal essential information about the interactions. The differential cross-section (DCS) throws light on the probability of scattering into a particular solid angle, which helps understand the directional scattering. In contrast, the total / Integral cross section (ICS) is the integral of DCS over all solid angles, which gives the overall interaction of the electron beam with the target.

Electrons have also been seen to possess orbital angular momentum (OAM). When such electrons possessing particular OAM are directed into a beam, the beam then acquires the same OAM as the electrons. Such beams are known as twisted/vortex electron beams. They are composed of both transverse and longitudinal momentum vector/wave vector components; the longitudinal wavevector causes the beam to propagate along the beam axis, and the transverse component spreads it radially outward perpendicular to the axis. Such beams house a line of singularity on the beam axis. The most natural twisted beam is the Bessel beam. Bessel beams are solutions to the Helmholtz equation in cylindrical coordinates. In this article, we study the interaction of Bessel beams possessing various OAM with molecules. Figure 1. shows different views of Bessel Beam specifically: (a) lateral view of the beam and (b) the cross-sectional view, and (c) the intensity profile of the generalized Bessel Beams (Fourier Transform) as discussed in the next section.

The study of twisted electron beams with matter has attracted increased research interest, as it has shown promising applications in high-resolution imaging [1], manipulation of nanoparticles by tweezing [2], and quantum communication[3]. Twisted beams have additional degrees of freedom owing to their orbital angular momenta, enabling them to act as higher information containers (qubits, qutrits, qudits, etc.). The helical motion of the twisted electrons with time produces large magnetic fields along the propagation axis. Having control over the beam size, very high magnetic fields may be generated at the nano-scale [4]. In addition, magnetic fields can interact with magnetic moments and thus can be used to characterize the magnetic properties of the targets under consideration. To realize these applications, it is essential to understand the nature and dynamics of the interaction between twisted electron beams and matter.

Ionization studies of twisted electron beams with atoms and small molecules such as the H and He atoms,  $H_2$ ,  $H_2O$ ,  $CH_4$ , and  $NH_3$  molecules are reported in the literature [5–8]. Theoretical studies on the elastic scattering of twisted beams have been reported for atomic targets [9, 10], and diatomic molecules with the example of  $H_2$  molecule [11]. The computations on the  $H_2$  molecule report cross-sections only at parallel and perpendicular orientations to the beam using Yukawa potentials. Experimentally, the study has yet to be performed on the elastic scattering of molecules by twisted electrons.

Computing the cross sections of many-electron atoms and molecules poses significant challenges while calculating ground state wavefunctions and electron correlation exactly. In addition, the integrals involving the wavefunctions and their overlap are formidable. None of the theoretical studies have involved an all-active electron approach and used the nuclear center's contribution to calculating Coulomb direct potentials.

Addressing the above challenges and the gaps, this article lays down the methodology to compute the differential

\* Also at Department of Physics, Birla Institute of Technology and Science, Pilani, Pilani Campus 333-031 (India)

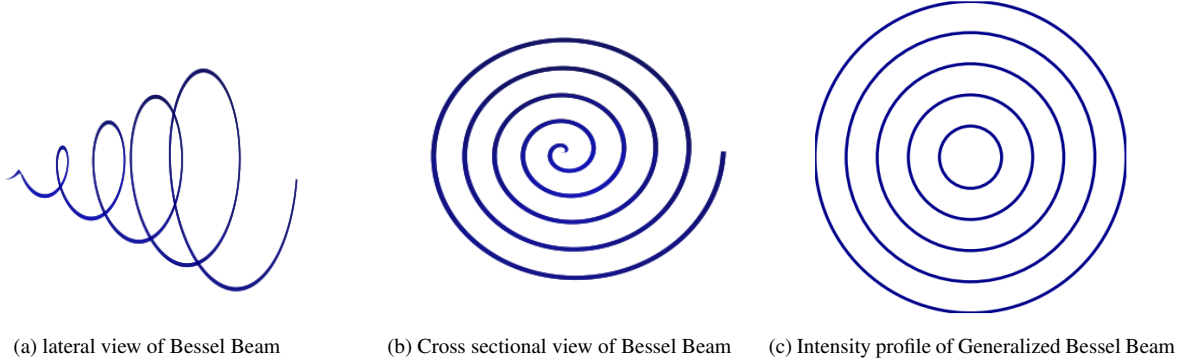


FIG. 1: Bessel Beams

and integral cross-sections of twisted electrons for polyatomic molecules with the example of the  $\text{CO}_2$  molecule. We compute the electronic wavefunctions and electron density using the Coupled-Cluster Singles and Doubles CCSD method. We go further by using multicentered wavefunctions and including the contribution of all the electrons in the molecule, their correlations, and the nuclear attractive potentials in the computation of the Coulomb direct potential. This direct potential is then used to compute the cross-sections. The computation of the cross sections for the twisted electron beam involves intricate calculations given in this article.

## II. THEORETICAL FORMALISM

This section lays out the formalism that is spread out into four subsections. The first is modeling the monochromatic Bessel beam, the second is modeling the target molecules, the third is the computational methodology used, and the fourth is the scattering amplitudes and cross-sections.

### A. Monochromatic Bessel Beam

A monochromatic Bessel electron beam is a Bessel beam of electrons that possesses a definite wavevector  $\mathbf{k}_i^{tw}$  which, in terms of its Cartesian components, is given as:

$$\mathbf{k}_i^{tw} = \mathbf{k}_{i\parallel} + \mathbf{k}_{i\perp} \quad (1)$$

where  $\mathbf{k}_{i\parallel}$  is the longitudinal wavevector, and  $\mathbf{k}_{i\perp}$  is the transverse wavevector. They individually are given as:

$$\mathbf{k}_{i\parallel} = k_z \hat{z} = (k_i \cos \theta_p) \hat{z} \quad (2)$$

$$\mathbf{k}_{i\perp} = (k_i \sin \theta_p \cos \phi_p) \hat{x} + (k_i \sin \theta_p \sin \phi_p) \hat{y} \quad (3)$$

Here,  $\theta_p$  and  $\phi_p$  are the polar and azimuthal angles of  $\mathbf{k}_i^{tw}$ . The beam can be described as a superposition of plane waves, each with longitudinal and transverse momentum components. The transverse momentum leads to the beam's divergence from the propagation axis. The expression for the Bessel

beam propagating along the  $z$ -axis in the positive  $z$ -direction in cylindrical coordinates is given by:

$$\psi_{\mathbf{k}_i m_l}^{(tw)} (r, \phi, z, b,) = J_{m_l}(k_{i\perp} r) e^{ik_{i\parallel} z} e^{im_l \phi} e^{-i\mathbf{k}_i \cdot \mathbf{b}} \quad (4)$$

where  $J_{m_l}$  is the Bessel function of order  $m_l$ , it is a function of the transverse component of the wavevector and radial coordinate.  $e^{ik_{i\parallel} z}$  is the plane-wave component, where  $k_{i\parallel}$  is the magnitude of the longitudinal component of the wavevector.  $e^{im_l \phi}$  is the azimuthal phase, with  $m_l$  being the topological charge, which is exactly equal to the order of the Bessel function.  $e^{-i\mathbf{k}_i \cdot \mathbf{b}}$  is the phase containing the effect of impact parameter  $\mathbf{b}$ .

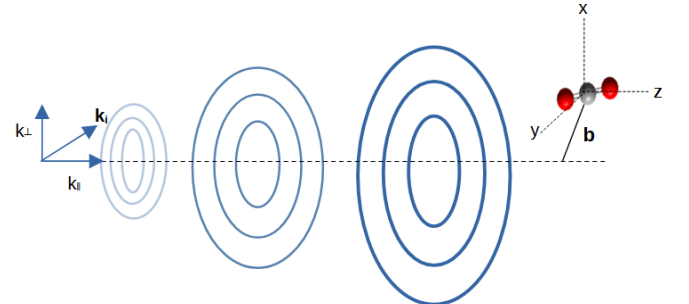


FIG. 2: A Bessel beam scattered of a triatomic molecule

To subdue the effect of particular beam orientations, we consider a generalized Bessel beam and work in the Fourier basis. This is shown in figure 1 (c) where the intensity profile is as though it uniformly impacts the target (without a  $\phi$  dependence). The Fourier-transform of (4) is given by:

$$\psi_{zm_l}^{(tw)} (\mathbf{r}) = \int_0^\infty \frac{d^2 k_{i\perp}}{2\pi} k_{i\perp} \int_0^{2\pi} \frac{d\phi_p}{2\pi} a_{zm_l}(\mathbf{k}_{i\perp}) e^{i\mathbf{k}_i \cdot \mathbf{r}} \quad (5)$$

while the Fourier amplitude of the twisted wavefunction is given by:

$$a_{zm_l}(\mathbf{k}_{i\perp}) = \sqrt{\frac{2\pi}{\kappa}} (-i)^{m_l} e^{im_l \phi_p} \delta(k_{i\perp} - \kappa) \quad (6)$$

$\varkappa$  is the transverse component of the wavevector. The Dirac delta function picks out the value  $\varkappa$  in Equation (5). The momentum transfer of the Bessel beam interaction is given by  $\Delta^{tw} = \mathbf{k}_i^{tw} - \mathbf{k}_s$ . Its magnitude in terms of the scattering angle ( $\theta_s$ ) can be deduced as:

$$\Delta^{tw} = 2k \sin(\theta_{ps}/2) \quad (7)$$

where  $\theta_{ps}$  is the angle between  $\mathbf{k}_i^{tw}$  and  $\mathbf{k}_s$ . It is calculated as follows:

$$\theta_{ps} = \cos^{-1} [\cos \theta_p \cos \theta_s + \sin \theta_p \sin \theta_s \cos \phi_p] \quad (8)$$

Here,  $\phi_s = 0$  because we consider a coplanar asymmetric geometry.

The expressions for the initial and final state wavefunctions are given by:

$$\langle \mathbf{r} | \psi_i \rangle = \psi_{zm_l}^{(tw)}(\mathbf{r}) \psi_m(\mathbf{r}) \quad (9)$$

$$\langle \mathbf{r} | \psi_f \rangle = \psi_{zm_l}^{(tw)}(\mathbf{r}) \psi_n(\mathbf{r}) \quad (10)$$

$\psi_{zm_l}^{(tw)}(\mathbf{r})$  is the incident twisted beam wavefunction (here, Bessel Beam), and  $\psi_m(\mathbf{r})$  and  $\psi_n(\mathbf{r})$  are the normalized initial and final molecular wavefunctions.

## B. Modeling Target Molecules

We model the target molecule using the active role of all electrons and the nuclear attractive potentials. We use the correlation-consistent quadruple zeta basis set cc-pVQZ to model the wave functions that include electron correlations. Many articles state using cc-pVQZ basis set [12–14]. This basis set employs 14 functions for each atomic orbital. To obtain the ground state of the target wave function, a geometry optimization coupled cluster CCSD calculation is performed in GAUSSIAN (G09) [15] requesting the output of a wavefunction file (.wfn file). We explicitly specify using all the electrons in GAUSSIAN for the CCSD calculations.

CCSD is a post-Hartree Fock method used to compute the ground state wavefunction, which particularly includes electron correlations. Hartree-Fock inherently neglects electron correlations. Many studies have used the CCSD method to obtain the ground state [16]. The correlations are brought about by operating the exponential powers of cluster operators[17], wherein the ansatz used is this exponential cluster operator with Hartree Fock wavefunctions and is given by:

$$\Psi_{cc} = e^{iT} \Phi_0 \quad (11)$$

where  $\Phi_0$  is the Hartree Fock wavefunction obtained after the Hartree Fock Calculation,  $\Psi_{cc}$  is the coupled cluster wavefunction, and  $T$  is the Cluster operator. The cluster operator

is an infinite operator involving various second quantization excitation operators[17].

CCSD uses single and double excitations to arrive at a highly accurate electronic structure of molecules. This is crucial to obtain the ground state required of the molecules for this study. Note that the excitations that CCSD uses are only those to compute the ground state wavefunctions and are unrelated to the main study of elastic scattering interactions of this study. This method is a wavefunction theory (WFT) method that computes the electron correlations exactly as opposed to Density Functional theory (DFT), which uses density functionals to compute the electron correlations.

The CCSD calculations yield a .wfn file, which is then analyzed by Multiwfn, a code developed by Lu et al. [18]. We use Multiwfn to extract the electron density as a function of the spatial coordinate points provided. The density is then used to calculate the elastic scattering form factor, which is given in the following subsections.

In this study, we model the  $CO_2$  molecule.  $CO_2$  is linear, with 22 electrons lacking a permanent dipole moment. It is also a greenhouse gas.

## C. Cross-sectional computation details

We have obtained the expressions for the projectile and the target in the previous subsections. We use these to compute cross-sections. We use the right-handed coordinate system to do so, with all calculations performed in atomic units. Gauss-Legendre quadrature has been used to compute the spherical coordinate integrals, with the number of sample points  $N = 12$  for each coordinate. The origin of the coordinate system is assumed to be at the molecule's center of mass (COM). The three nuclei are the three centers of the molecular wavefunctions.

Experimentally, orienting a molecule in a particular direction is extremely challenging. This leads to experimental studies yielding randomly oriented cross-sections that tend to be orientation averaged. To obtain orientation-averaged cross-sections theoretically, we perform a passive rotation of the incident and scattered vectors, keeping the molecular orientation fixed. This rotation is done incrementally, spanning all solid angles. We denote these increments by  $\theta_1$  and  $\phi_1$ . The momentum transfer vector is automatically rotated incrementally by these constant angles. Figure 3 depicts the orientation averaging where  $k_i$  is incremented by  $10^\circ$ . The symbol near  $\phi_1$  implies that the rotation is into the plane of the paper. The molecule could have any shape (shown here as spherical, just as an example).

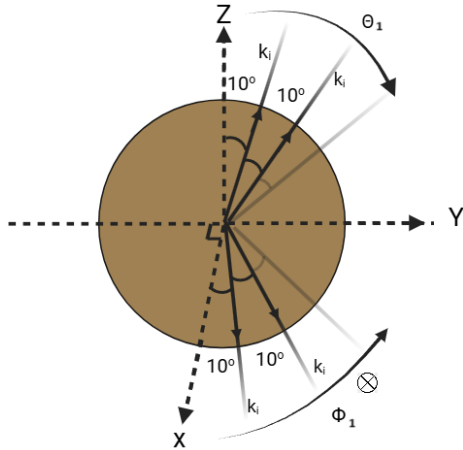


FIG. 3: Varying incident electron beam direction keeping molecule's orientation fixed with respect to coordinate axes

The cross-sections are calculated for each configuration and are averaged. We have used an increment of  $\theta_1$  and  $\phi_1$  being  $10^\circ$  each.  $\theta_1$  and  $\phi_1$  are explicitly used in the formalism in the following subsections.

#### D. Scattering Amplitudes

Here, we provide a formalism for angle-resolved differential scattering amplitude calculations for the orientation averaged system in the first Born Approximation. The Coulomb direct interaction potential between the incident electron and target molecule is:

$$V_d = - \sum_{i=1}^M \frac{Z_i}{|\mathbf{r}_0 - \mathbf{r}_i|} + \sum_{j=1}^N \frac{1}{|\mathbf{r}_0 - \mathbf{r}_j|} \quad (12)$$

Here,  $i$  is summed over the  $M$  nuclear centers each having charge  $Z_i$  and position vector  $\mathbf{r}_i$  producing an attractive potential.  $j$  is summed over the  $N$  molecular electrons, each having charge -1 and position vector  $\mathbf{r}_j$  producing a repulsive potential.  $\mathbf{r}_0$  are the coordinates of the incident projectile. Since we work at sufficiently high energies, the exchange interactions are negligible, and we ignore their contributions. For  $CO_2$ ,  $M = 3$  and  $N = 22$ .  $M$  and  $N$  vary with molecules.

The elastic scattering transition matrix element/scattering amplitude in terms of the initial state, final state, and direct potential  $V_d$  (Equation (14)) in the first Born Approximation is:

$$T_{fi} = \langle \psi_f | V_d | \psi_i \rangle \quad (13)$$

$\psi_i$  and  $\psi_f$  are the composite initial and final wavefunctions (Equations (1) and (2) or Equations (8) and (9) respectively). Because we consider elastic scattering, the initial and final states change only in direction. Hence we can represent them both by the state  $|i\rangle$ . Therefore,

$$T_{ii} = V_{ii} = \langle i | V_d | i \rangle = - \sum_{j=1}^M Z_j \int \frac{e^{i\Delta \cdot \mathbf{r}_0}}{|\mathbf{r}_0 - \mathbf{l}_j|} \int \rho(\mathbf{r}) d\mathbf{r} + \int \int \frac{\rho(\mathbf{r}) e^{i\Delta \cdot \mathbf{r}_0}}{|\mathbf{r}_0 - \mathbf{r}|} d\mathbf{r}_0 d\mathbf{r} \quad (14)$$

$\mathbf{r}_0$  are the coordinates of the projectile,  $\mathbf{l}_j$  is the position vector of each nucleus, and  $\mathbf{r}$  are the coordinates of the molecule. The density of the molecule as a function of spatial coordinates is given in terms of the inner products of the molecular wavefunctions  $\psi_n$  and  $\psi_m$ . Because we assume that the molecular wavefunctions do not change,  $m = n$  and therefore:

$$\rho(\mathbf{r}) = |\psi_m(\mathbf{r})|^2 = \sum_i \eta_i \left| \sum_{\mu} C_{\mu,i} \beta_{\mu}(\mathbf{r}) \right|^2 \quad (15)$$

where the electron density equals the sum of the orbitals times their occupation number  $\eta_i$ .  $i$  is the index of the orbitals. The orbitals are given by a mod square of the sum over  $\mu$  of the orbital coefficients  $C_{\mu,i}$  times the basis function  $\beta_{\mu}(\mathbf{r})$ .  $\mu$ , the index of the basis functions of the orbitals, and  $C_{\mu,i}$  corresponds to the coefficient of the  $i^{th}$  orbital and  $\mu^{th}$  basis function.

##### 1. Plane-wave scattering amplitude

The magnitudes of the wavevectors for plane wave elastic scattering are  $k_i = k_s = k$ . The momentum transfer of this interaction is given by  $\Delta = \mathbf{k}_i - \mathbf{k}_s$ . Its magnitude in terms of the scattering angle  $\theta_s$  can be deduced to have the value:

$$\Delta = 2k \sin(\theta_s/2) \quad (16)$$

On simplifying Equation (16) using Bethe's integral given in [19, 20], we obtain the plane wave scattering amplitude as:

$$T_{ii}^{pw}(\Delta) = - \frac{2}{\Delta^2} (\alpha - \chi) \quad (17)$$

$\alpha$  is the contribution of the attractive potential experienced by the incoming electron by the  $M$  nuclear centers.  $\alpha$  in terms of the  $j^{th}$  nuclear center having position vector  $\mathbf{l}_j$  is given by:

$$\alpha = \sum_{j=1}^M Z_j \exp(i\Delta \cdot \mathbf{l}_j) \quad (18)$$

$\alpha$  brings in the nuclear centers' contribution where  $Z_j$  is the positive charge that the  $j^{th}$  nucleus carries. For  $CO_2$ , Equation (19) reads:

$$\alpha = 8 \exp(il_1 \Delta \cos(\theta_{\Delta} + \theta_1)) + 8 \exp(-il_1 \Delta \cos(\theta_{\Delta} + \theta_1)) + 6 \quad (19)$$

which simplifies to:

$$\alpha = 16 [\cos(l_1 \Delta \cos(\theta_\Delta + \theta_1))] + 6 \quad (20)$$

$l_1$  is the modulus of magnitudes of the position vectors of the Oxygen nuclei and is obtained to be 2.145 a.u. The carbon nucleus is at the origin of our coordinate system.  $\theta_1$  is added, which accounts for the angular increment in  $\theta_\Delta$  as the system is orientation averaged.

To evaluate  $\Delta \cdot l_j$  the angle between  $\Delta$  and  $l_j$  with the fixed coordinate axes is required.  $\theta_\Delta$  is the angle that  $\Delta$  makes with the coordinate axes and is given by:

$$\theta_\Delta = \cos^{-1} \left( \frac{k}{\Delta} (1 - \cos \theta_s) \right) \quad (21)$$

Because the molecules lie on the z-axis, the angle made by the nuclear center's position vector with the z-axis  $\theta_{l_j} = 0^\circ$

The rightmost double integral of Equation (15) simplifies to  $\chi$  the target's elastic scattering form factor given by[19]:

$$\chi = \int \exp(i\Delta \cdot \mathbf{r}) \rho(\mathbf{r}) d\mathbf{r} \quad (22)$$

The electron density  $\rho(\mathbf{r})$  as a function of the spatial coordinates  $r$ ,  $\theta$ , and  $\phi$  is introduced into the code from the output of Multiwfn.

The cosine of the angle between  $\Delta$  and  $\mathbf{r}$  to be used in (25) is given by:

$$\begin{aligned} \cos(\theta_{\Delta r}) &= \cos(\theta_\Delta + \theta_1) \cos \theta + \sin(\theta_\Delta + \theta_1) \sin \theta \\ &\cos(\phi - \phi_1) \end{aligned} \quad (23)$$

Here,  $\theta_1$  and  $\phi_1$  account for the angular increment in  $\theta_\Delta$  as the system is orientation averaged.

## 2. Bessel scattering amplitude

The twisted scattering amplitude/transition matrix elements of the molecule are given in terms of plane wave scattering amplitude/matrix elements as follows:

$$T_{ii}^{tw}(\varkappa, \Delta^{tw}) = (-i)^{m_l} \int_0^{2\pi} \frac{d\phi_p}{2\pi} e^{im_l \phi_p} T_{ii}^{pw}(\Delta^{tw}) \quad (24)$$

Note that  $T_{ii}^{pw}$  in the integrand is a function of  $\Delta^{tw}$ . The angles  $\Delta^{tw}$  with fixed coordinate axes are:

$$\theta_{\Delta^{tw}} = \cos^{-1} \left( \frac{k}{\Delta^{tw}} (\cos \theta_p - \cos \theta_s) \right) \quad (25)$$

and,

$$\phi_{\Delta^{tw}} = \cos^{-1} \left[ \frac{k(\sin \theta_p \cos \phi_p - \sin \theta_s)}{\Delta^{tw} \sin \theta_{\Delta^{tw}}} \right] \quad (26)$$

Note that, for the Bessel beam  $\Delta$  in the Equations (20)-(25) must be replaced by  $\Delta^{tw}$ .

The cosine of the angle between  $\Delta^{tw}$  and  $\mathbf{r}$  to be used in (25) is given by:

$$\begin{aligned} \cos \theta_{\Delta^{tw} r} &= \cos(\theta_{\Delta^{tw}} + \theta_1) \cos \theta + \sin(\theta_{\Delta^{tw}} + \theta_1) \sin \theta \\ &\cos(\phi - \phi_{\Delta^{tw}} - \phi_1) \end{aligned} \quad (27)$$

These are the only modifications that change while calculating  $\alpha$  and  $\chi$  in Equation (18) for the Bessel scattering amplitude.

## E. Cross-Sections

Once  $T_{ii}$  for plane waves or twisted waves is obtained, the differential and integral cross-sections can be obtained as follows:

### 1. Differential cross-sections

The plane wave differential cross-section is given by:

$$\left( \frac{d\sigma}{d\Omega} \right)^{pw} = |T_{ii}^{pw}|^2 \quad (28)$$

The twisted wave differential cross-section for particular values of  $m$  is given by:

$$\left( \frac{d\sigma}{d\Omega} \right)^{tw} = |T_{ii}^{tw}|^2 \quad (29)$$

To yield experimentally realizable results, we average the differential cross-section over all impact parameters. The averaging considers the number of target molecules tending to  $\infty$ . This averaging is performed in addition to the orientation averaging. This differential cross section does not depend on the topological charge of the beam but rather only on its opening angle  $\theta_p$  [10, 21].

$$\left( \frac{d\sigma(\Delta)}{d\Omega} \right)_{av}^{tw} = \frac{1}{2\pi \cos \theta_p} \int_0^{2\pi} d\phi_p \left( \frac{d\sigma(\Delta^{tw})}{d\Omega} \right)^{pw} \quad (30)$$

### 2. Integral cross section (ICS)

The integral (total) elastic cross sections for all the above cases of plane and twisted waves are obtained by integrating over all solid angles of the scattered electron.

$$\sigma = \int \frac{d\sigma}{d\Omega} d\Omega = 2\pi \int_0^\pi d\theta_s \sin \theta_s \left( \frac{d\sigma}{d\Omega} \right) \quad (31)$$

### III. RESULTS AND DISCUSSIONS

#### A. Plane-wave Elastic Differential Cross Section

The results for the plane wave absolute elastic electron differential cross section for carbon dioxide are presented in this subsection. The results are plotted for intermediate incident electron energies ranging from 300eV to 1keV. We note that we have not evaluated the differential cross sections at the singular point  $\theta_s = 0^\circ$  as the cross sections blow up. This is because we use Bethe's integrals, and the approach used fails as  $\theta_s \rightarrow 0$ . The cross sections presented are from  $\theta_s = 1^\circ$ .

Figure 4 depicts four subplots of each differential cross sec-

tion plotted against the scattering angle  $\theta_s$  for the plane wave electron impact. Subfigures (a), (b), (c), and (d) show the results for  $E_i = 300\text{eV}$ ,  $500\text{eV}$ ,  $800\text{eV}$ , and  $1\text{keV}$ , respectively. A continuous blue curve represents the present model. The red points represent experimental results obtained from the literature.

The experimental data points are obtained from Iga et al. (1999) [22] for  $E_i = 300\text{eV}$ , whereas for  $E_i = 500\text{eV}$ ,  $800\text{eV}$ , and  $1\text{keV}$  by Iga et al. (1984) [23]. The results of our theoretical model match the experimental data obtained by Iga et al.(1984) at  $E_i = 500\text{eV}$ ,  $800\text{eV}$ , and  $1\text{keV}$ . However, there is some deviation for  $E_i = 300\text{eV}$  from that of Iga et al.(1999).

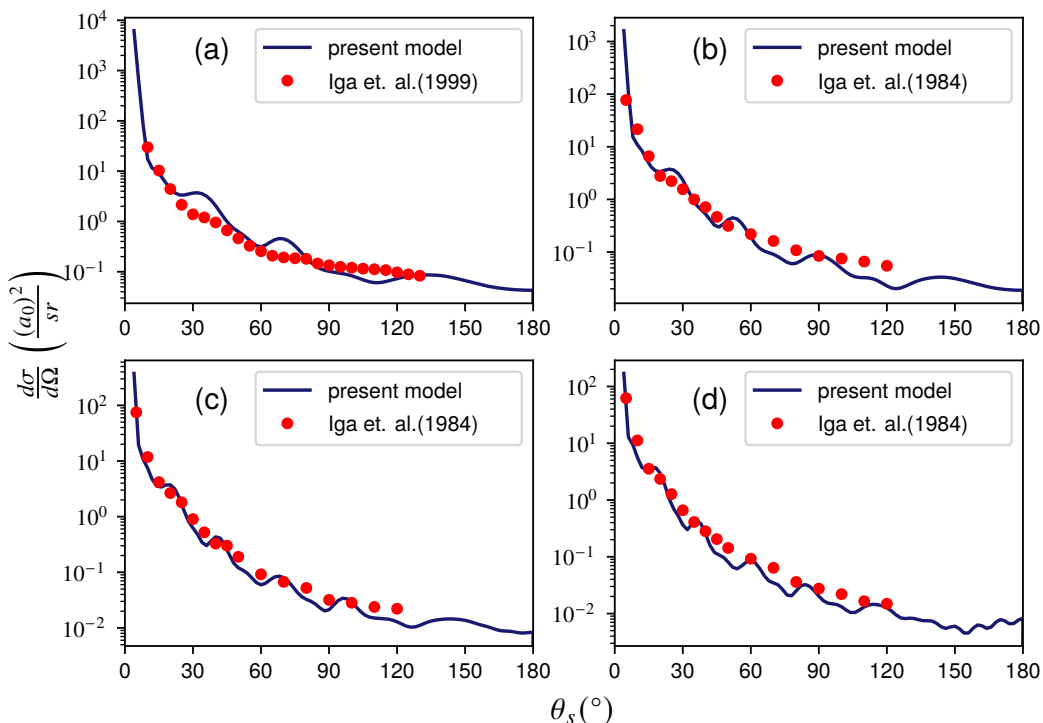


FIG. 4: Absolute elastic differential cross sections for plane wave electron impact on  $CO_2$ . Incident energy: (a) 300eV, (b) 500eV (c) 800eV (d) 1keV. The points represented by red dots are experimental values obtained by Iga et al. [22, 23]

The differential cross sections for elastic scattering of plane waves show deviations from a smooth descending curve. This is due to the multicentered effects considered. The three nuclear centers act as three sources of waves, and thus, we get similar to Young's triple slit interference pattern modulated on the smooth decay. With the theoretical results, one can observe pairs of maxima that repeat and correspond to the primary and secondary maxima of triple-slit interference. The results obtained by our model are in good agreement with the published experimental data. The good agreement of the results of our model with those of the experimental data establishes that our model can determine with sufficient accuracy the elastic differential cross sections for plane waves at

the intermediate energies 300eV, 500eV, 800eV, and 1keV. We now use the benchmarked model to study the interactions of the monochromatic Bessel beam with molecular targets in this model.

#### B. Twisted-wave elastic differential cross-section

Here, we present the results of the twisted Bessel electron beam impact elastic differential cross section for  $CO_2$  molecule at intermediate energies ranging from 300eV to 1keV. These results are divided into DCS as a function of OAM and impact parameter averaged DCS.

### 1. Differential Cross Section as a function of OAM

This subsection presents the results for twisted electron impact absolute elastic differential cross sections for topological charges  $m_l = 1, 2$ , and  $3$  at impact parameter  $b = 0$ . The opening angle used for these calculations is  $\theta_p = 10^\circ$ . As a reference, the plane wave results are also shown.

Figure 5 depicts four subplots of each differential cross section plotted against the scattering angle  $\theta_s$  for Bessel wave electron impact on carbon dioxide molecule. Subfigures (a), (b), (c), and (d) in the figure depicts the results for  $E_i = 300\text{eV}$ ,  $500\text{eV}$ ,  $800\text{eV}$ , and  $1\text{keV}$ , respectively. A solid dark blue curve represents the plane wave DCS. The twisted DCS for different

$m_l$  are shown in lighter colors.

We note that for incident energy  $E_i = 300\text{eV}$ , the twisted DCS peaks at the opening angle of  $\theta_p = 10^\circ$  with the value of  $10^4 a_0^2$ . We report that the value of DCS approaching the singular point  $\theta_s = 0^\circ$  tends to 0 rather than  $\infty$  as compared to the plane wave case. We have not plotted the DCS at the singular point  $\theta_s = 0^\circ$  as the range on the y-axis would be too high, suppressing important features in the graph. For higher topological charges, the DCS beyond  $\theta_s = 30^\circ$  is less than that for lower topological charges. In all cases, the DCS exhibits an oscillating behavior. The peak amplitude decreases for higher incident energies when the energy is increased from  $300\text{eV}$  to  $1\text{keV}$  as shown in subplots (a) to (d).

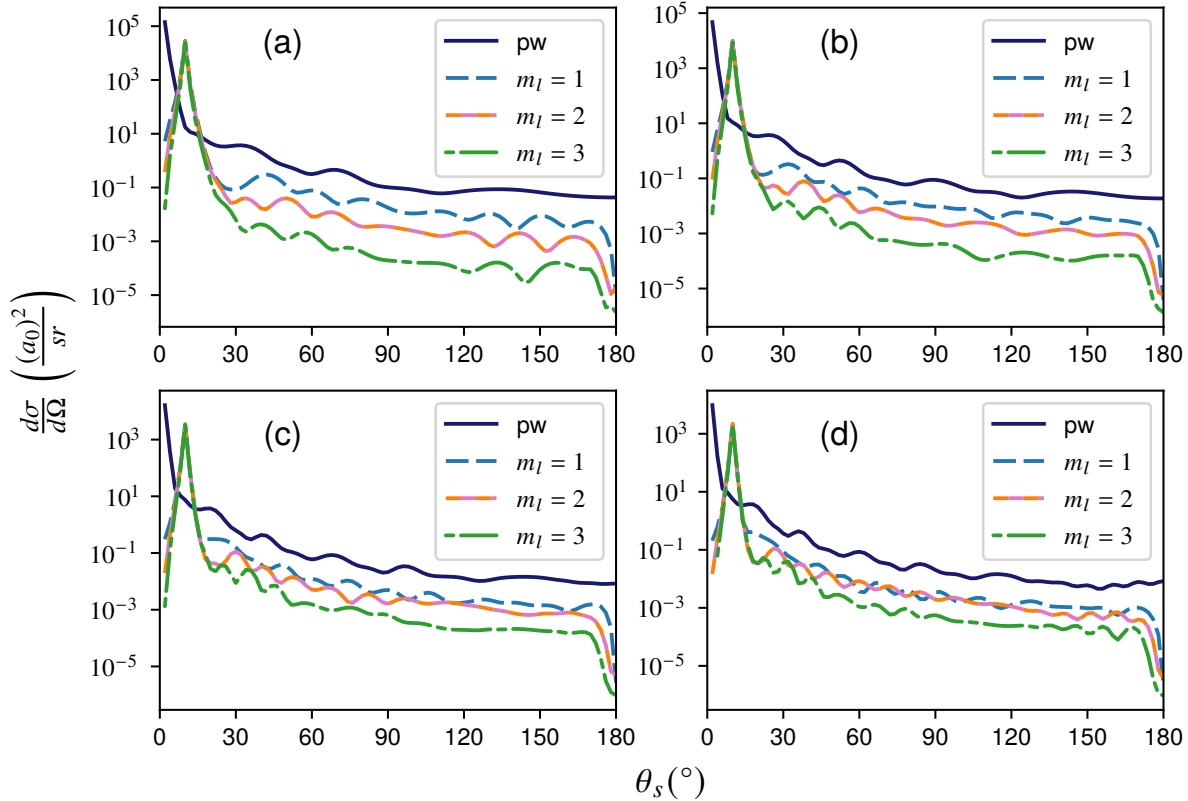


FIG. 5: OAM dependent differential cross section of Bessel beam impact on  $CO_2$  molecule at energies (a)  $300\text{eV}$ , (b)  $500\text{eV}$ , (c)  $800\text{eV}$  and (d)  $1\text{keV}$

The peak amplitude of the DCS at  $300\text{eV}$  is greater than that at  $1\text{keV}$  by one order of magnitude; that is, the peak amplitude is of the order of  $10^4 a_0^2$  at  $300\text{eV}$  and just below  $10^3 a_0^2$  at  $1\text{keV}$ . This can be understood by looking at Equation (6). As the energy increases, the transverse component  $\varkappa$  of the Bessel beam also increases, and the  $\varkappa$  sitting in the denominator reduces the magnitude of the DCS. We also observe that the peak becomes slightly narrower as the energy is increased from  $300\text{eV}$  to  $1\text{keV}$ . This can be explained as when the transverse component  $\varkappa$  of the wavevector, present as the argument of the

Bessel function increases, the Bessel function squishes, and the maxima of the Bessel function narrows. Hence pushing the scattered electrons into a narrower solid angle. However, the DCS of the target by twisted electron beam impact is much lower than the plane wave results apart from the peak. The differential cross section reported is the smallest for  $m_l = 3$  and highest for  $m_l = 1$ . This is again due to the behavior of the Bessel function's maxima, the maximum of  $J_3 < J_2 < J_1 < J_0$ .

The peak amplitude at  $\theta_s = 10^\circ$  is the same for all topological charges in all graphs in Figures. The DCS seems to merge

as energy increases from 300eV to 1keV. For large incident energies, for e.g., at 1keV, the DCS values of the three topological charges merge, particularly for  $m_l = 1$  and  $m_l = 2$ . It is difficult to differentiate between  $m_l = 1$  and  $m_l = 2$  at 1keV. A smooth decay of the DCS is presented by Koshelava et al. [9] for atomic systems. This is contrary to what we see in the DCS. That is, we see many fluctuations. The oscillations are due to the interference effects of electron waves that are obtained from the centers. We also note that the maxima for plane-wave and  $m_l=2$  are in phase and are exactly out of phase with  $m_l=1$ . This is due to the inherent phase difference of  $\pi$  between the Bessel beams with consecutive topological charges and a phase difference of 0 between alternate topological charges at points that are in the plane perpendicular to the axis.

## 2. Impact Parameter Averaging

In this subsection, we present the macroscopic experimentally obtainable differential cross sections, also known as the impact parameter-averaged differential cross section. It represents the beam impacting an infinite number of target molecules uniformly distributed transversely, resembling experimental situations. Hence, they are called cross-sections for macroscopic targets of molecules. Here, we present the above for  $CO_2$  molecule with opening angles  $\theta_p = 6^\circ$ ,  $20^\circ$ , and  $45^\circ$ . Plane-wave results are also shown for comparison.

Figures 7 depict four subplots of each impact parameter averaged differential cross section plotted against the scattering angle  $\theta_s$  for Bessel electron beam impact on  $CO_2$  molecule. Subfigures (a), (b), (c), and (d) show the results for  $E_i = 300\text{eV}$ ,  $500\text{eV}$ ,  $800\text{eV}$ , and  $1\text{keV}$ , respectively. The solid dark blue curve shows the plane wave DCS. The twisted DCS for different  $\theta_p$  values is shown in magenta, light blue, and green.

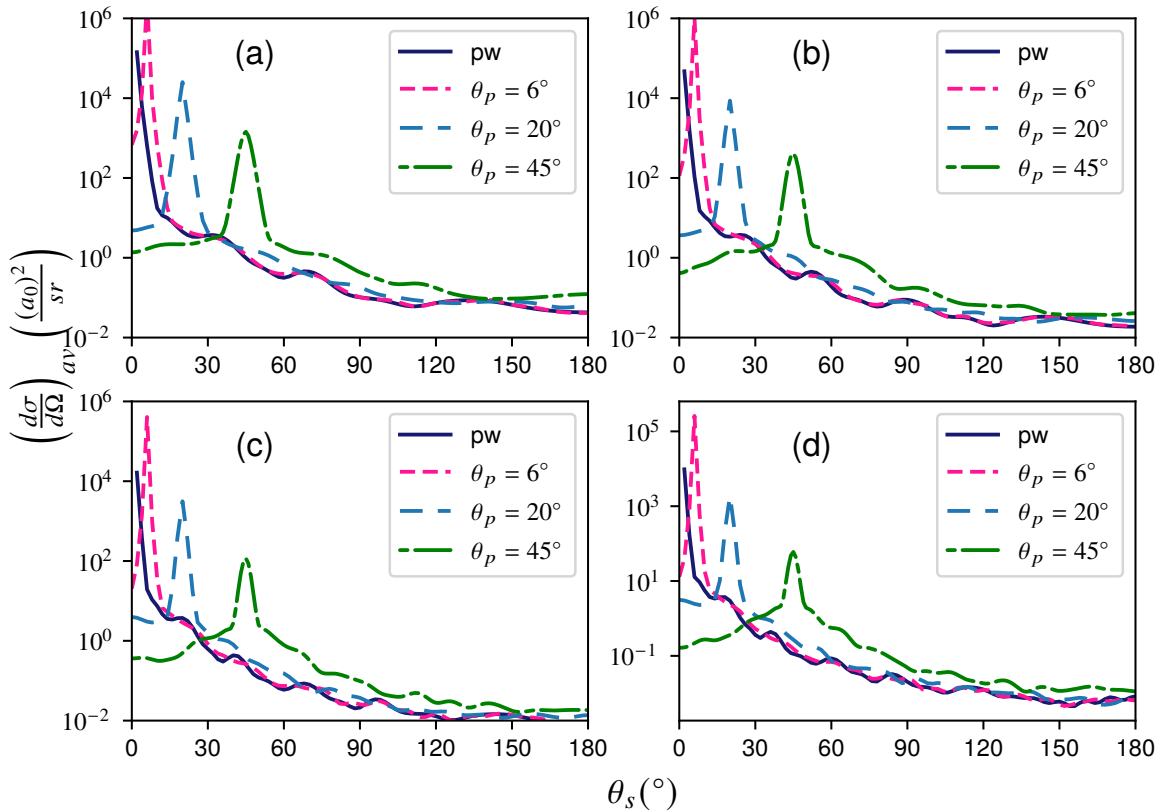


FIG. 6: Impact parameter averaged Bessel Differential Cross-Section for  $CO_2$  (a) 300eV, (b) 500eV, (c) 800eV and (d) 1keV

We observe peaks in the differential cross section at the given opening angles of  $\theta_p$  for energies  $E_i = 300\text{eV}$  to  $1\text{keV}$ . As  $\theta_p$  increases from  $6^\circ$  to  $45^\circ$ , the peak's value reduces. There are nearly two orders of magnitude difference between the peak value for  $\theta_p = 6^\circ$  and  $20^\circ$  and almost the exact difference between those for  $20^\circ$  and  $45^\circ$  for each incident energy. However, as the incident energy is increased from  $E_i = 300\text{eV}$  to  $1\text{keV}$ , the amplitudes of the peaks gradually decrease. The difference in the peak amplitude is nearly one order of magnitude at energies  $E_i = 300\text{eV}$  to  $1\text{keV}$ , i.e., from  $10^6 a_0^2$  to  $10^5 a_0^2$  and  $10^4 a_0^2$  to  $10^3 a_0^2$  for those corresponding to  $\theta_p = 6^\circ$  and  $20^\circ$ . However, for  $\theta_p = 45^\circ$ , it reduces by nearly two orders of magnitude,  $10^3 a_0^2$  to  $10^1 a_0^2$ . This can be explained by Equation (32), which strongly depends on  $\theta_p$  in the denominator; as  $\theta_p$  increases from  $6^\circ$  to  $45^\circ$ , the denominator decreases. Physically, this can be understood as, when  $\theta_p$  increases, the wavevectors  $\mathbf{k}_{i\parallel}$  decreases, whereas  $\mathbf{k}_{i\perp}$  increases. The decrease in  $\mathbf{k}_{i\parallel}$  implies the force exerted by the projectile on the target in the solid angle around  $\theta_p$  is reduced. This is seen from Equations (2) and (3). We see that as the opening angle increases, the magnitude of the peak of the DCS peaks at higher  $\theta_s$ . The DCS at higher  $\theta_s$ , as given in Equations (32) and (18), reduces due to  $\Delta^2$  present in the denominator, with  $\Delta$  being a function of  $\sin(\theta_s/2)$ . The twisted DCS nearly follows the plane wave DCS after  $\theta_s = 90^\circ$  with an oscillatory behavior as given by the triple slit interference pattern.

### C. Integral Elastic Cross Section (ICS)

The integral cross sections corresponding to the electron elastic scattering of  $CO_2$  molecules for various twisted electron topological charges and the beam's interactions with macroscopic molecular targets averaged over all impact parameters are presented in this section. Figure 7 depicts two subplots representing the integral cross-section plots of the target molecules by the twisted Bessel beam impact, which depend on the topological charges and opening angle  $\theta_p$ , respectively. The plane wave integral cross sections are also plotted for reference and represented by a continuous dark blue curve. The integral cross-sections are plotted as a function of incident energies where the DCS is integrated over  $\theta_s$  according to Equation (34).

We note that the DCS of the plane waves blows up in the forward direction, leading to the blowing up of the integral cross-section. Hence, the DCS are integrated from  $5^\circ$  to  $180^\circ$  for both the OAM-dependent and macroscopic target cases. The blowing up of the integral cross section is due to the blowing up of the differential cross section as  $\theta_s \rightarrow 0^\circ$ . In addition, we have plotted integral cross-sections from  $E_i = 10\text{eV}$  to  $E_i = 1\text{keV}$ . For  $E_i \rightarrow 0$ , the momentum transfer  $\Delta \rightarrow 0$ , blows up the scattering amplitude given by (18); hence, we report results above  $E_i = 10\text{eV}$ , resulting in our model not accurately predicting the features at lower energies. This is also due to the Born approximation failing at lower energies, the plane waves representing the incident, and scattered electrons that do not agree at lower energies.

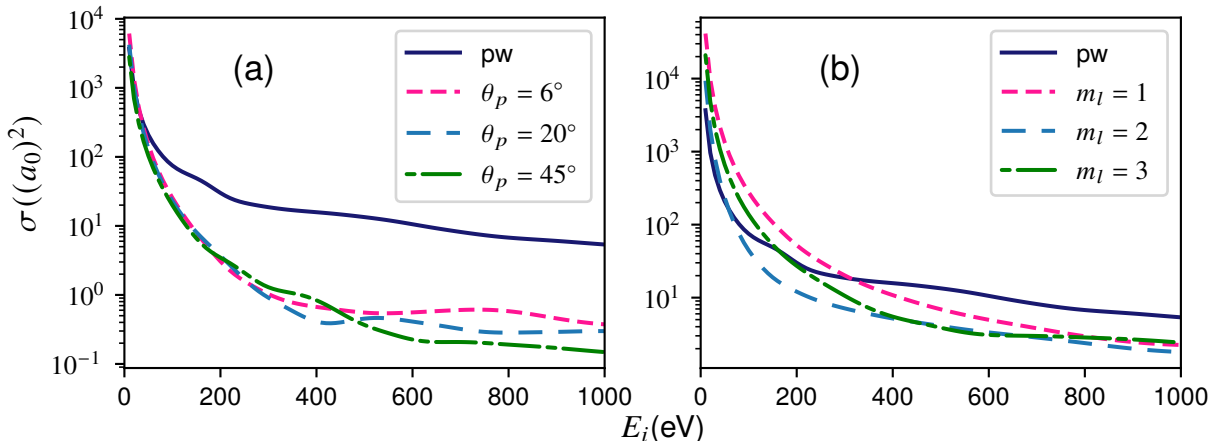


FIG. 7: Integral Elastic Cross-Section OAM dependent (a)  $CO_2$  and (b)  $N_2O$

Figure 7(a) depicts the ICS results for topological charges  $m_l = 1, 2$ , and  $3$ . The impact parameter used is  $\mathbf{b} = 0$ . We note that the integral cross-sections obtained for all three twisted topological charges have considerably lower values than the plane waves. This can also be inferred from the DCS of the twisted beams being lower than that of the plane waves in Figure 5. As shown in Figure 7 (a), the cross sections of the three topological charges decrease with energy and intertwine beyond  $250\text{eV}$ . The integral cross sections reach approximately

one order of magnitude at  $E_i = 1\text{keV}$ . Here, it is seen that for  $m_l = 1$ , the integral cross-section is the highest, while for  $m_l = 3$  is the least. Figure 7 (b) depicts the impact parameter-averaged ICS results as a function of incident energy  $E_i$  for macroscopic  $CO_2$  molecules. This implies that the beam impacts a large number of molecules. We see that, similar to plane waves, they decrease as the energy increases. The integral cross-sections of the twisted waves are nearly equal to or greater than the plane wave cross-sections. This can also be inferred from the DCS

plots in Figures 7 and 8 of the impact parameter averaging, where the twisted-wave DCS are greater in magnitude than those of the plane waves. As before, the impact parameter averaged ICS for  $CO_2$  for different  $\theta_p$  intertwines.

#### IV. CONCLUSIONS

We have presented a formalism and methodology to obtain accurate elastic differential and integral cross-sections of molecules by plane and Bessel electron beam impact theoretically with  $CO_2$  molecules as an example. We used post-Hartree Fock methods to obtain the ground state wavefunctions followed by the electron density, which brings about the effects of all molecular electrons in the cross-section, thus formulating the all-active electron approach. We also used a multicentered approach by considering three centers for each molecule. This methodology is a powerful approach to easily determine the cross-sections of complex molecular targets. We benchmarked our model for plane-wave experimental data and extended it

to the twisted wave case by investigating the cross-sections for OAM dependence and impact parameter averages. We have seen that the DCS depends on the OAM and the opening angle  $\theta_p$  of twisted beams. This method can be extended to inelastic scattering and ionization processes on other molecular targets to investigate the electronic structure. One could also investigate the scattering at low energies, where our model fails to be accurate.

#### V. ACKNOWLEDGMENTS

We acknowledge the Department of Science and Technology(DST), Government of India for funding received through the grant CRG/2021/003828.

#### VI. DATA AVAILABILITY

Data supporting this study's findings are available from the corresponding author upon reasonable request.

---

- [1] V. Grillo, J. Harris, G. C. Gazzadi, R. Balboni, E. Mafakheri, M. R. Dennis, S. Frabboni, R. W. Boyd, and E. Karimi, Generation and application of bessel beams in electron microscopy, *Ultramicroscopy* **166**, 48 (2016).
- [2] T. Shi and Z. Ding, Multislice method based full-space analysis on mechanical interaction of electron vortex beam with a crystalline particle, *Ultramicroscopy* **238**, 113551 (2022).
- [3] H. Larocque, I. Kaminer, V. Grillo, G. Leuchs, M. J. Padgett, R. W. Boyd, M. Segev, and E. Karimi, ‘twisted’electrons, *Contemporary Physics* **59**, 126 (2018).
- [4] V. Grillo, T. R. Harvey, F. Venturi, J. S. Pierce, R. Balboni, F. Bouchard, G. Carlo Gazzadi, S. Frabboni, A. H. Tavabi, Z.-A. Li, *et al.*, Observation of nanoscale magnetic fields using twisted electron beams, *Nature communications* **8**, 689 (2017).
- [5] N. Dhankhar, A. Mandal, and R. Choubisa, Double ionization of helium by twisted electron beam, *Journal of Physics B: Atomic, Molecular and Optical Physics* **53**, 155203 (2020).
- [6] N. Dhankhar and R. Choubisa, Triple-differential cross section for the twisted-electron-impact ionization of the water molecule, *Physical Review A* **105**, 062801 (2022).
- [7] N. Dhankhar, Neha, and R. Choubisa, Dynamics of twisted electron impact ionization of ch4 and nh3 molecule, *Atoms* **11**, 82 (2023).
- [8] M. Sahlaoui and M. Bouamoud, Cross sections for electron-impact ionization of water molecules, *Canadian Journal of Physics* **89**, 723 (2011).
- [9] V. Kosheleva, V. Zaytsev, A. Surzhykov, V. Shabaev, and T. Stöhler, Elastic scattering of twisted electrons by an atomic target: Going beyond the born approximation, *Physical Review A* **98**, 022706 (2018).
- [10] V. Serbo, I. Ivanov, S. Fritzsche, D. Seipt, and A. Surzhykov, Scattering of twisted relativistic electrons by atoms, *Physical Review A* **92**, 012705 (2015).
- [11] A. Maiorova, S. Fritzsche, R. Müller, and A. Surzhykov, Elastic scattering of twisted electrons by diatomic molecules, *Physical Review A* **98**, 042701 (2018).
- [12] V. Špirko, X. Li, and J. Paldus, Potential energy curve of n 2 revisited, *Collection of Czechoslovak Chemical Communications* **76**, 327 (2011).
- [13] Y. Pak, R. C. Woods, and K. A. Peterson, Coupled cluster prediction of vibrational band intensities for sif2 and pf2+, *The Journal of chemical physics* **106**, 8283 (1997).
- [14] J. Sánchez-Márquez, V. García, D. Zorrilla, and M. Fernández, On electronegativity, hardness, and reactivity descriptors: a new property-oriented basis set, *The Journal of Physical Chemistry A* **124**, 4700 (2020).
- [15] M. J. F. G. W. T. H. B. S. G. E. Scuseria, Gaussian09 revision e.01, gaussian Inc. Wallingford CT 2009.
- [16] S. Arulmozhiraja and T. Ohno, Ccsd calculations on c14, c18, and c22 carbon clusters, *The Journal of chemical physics* **128** (2008).
- [17] I. Y. Zhang and A. Grüneis, Coupled cluster theory in materials science, *Frontiers in Materials* **6**, 123 (2019).
- [18] T. Lu and F. Chen, Multiwfns: A multifunctional wavefunction analyzer, *Journal of computational chemistry* **33**, 580 (2012).
- [19] B. H. Bransden and C. J. Joachain, *Physics of atoms and molecules* (Pearson Education India, 2003).
- [20] R. Tweed, Double processes in e—he collisions, *Zeitschrift für Physik D Atoms, Molecules and Clusters* **23**, 309 (1992).
- [21] D. V. Karlovets, G. L. Kotkin, V. G. Serbo, and A. Surzhykov, Scattering of twisted electron wave packets by atoms in the born approximation, *Phys. Rev. A* **95**, 032703 (2017).
- [22] I. Iga, M. Homem, K. Mazon, and M. Lee, Elastic and total cross sections for electron-carbon dioxide collisions in the intermediate energy range, *Journal of Physics B: Atomic, Molecular and Optical Physics* **32**, 4373 (1999).
- [23] I. Iga, J. Nogueira, and L. Mu-Tao, Elastic scattering of electrons from co2 in the intermediate energy range, *Journal of Physics B: Atomic and Molecular Physics* **17**, L185 (1984).
- [24] R. A. Herring, A new twist for electron beams, *science* **331**, 155 (2011).

[25] N. Ray, M. Fleischmann, D. Weckbecker, S. Sharma, O. Pankratov, and S. Shallcross, Electron-phonon scattering and in-plane electric conductivity in twisted bilayer graphene, *Physical Review B* **94**, 245403 (2016).

[26] A. Harris, Projectile coherence effects in twisted electron ionization of helium, *Atoms* **11**, 79 (2023).

[27] S. N. Khonina, N. L. Kazanskiy, S. V. Karpeev, and M. A. Butt, Bessel beam: Significance and applications—a progressive review, *Micromachines* **11**, 997 (2020).

[28] V. Grillo, E. Karimi, G. C. Gazzadi, S. Frabboni, M. R. Dennis, and R. W. Boyd, Generation of nondiffracting electron bessel beams, *Physical Review X* **4**, 011013 (2014).

[29] K. Y. Bliokh, I. P. Ivanov, G. Guzzinati, L. Clark, R. Van Boxem, A. Béché, R. Juchtmans, M. A. Alonso, P. Schattschneider, F. Nori, *et al.*, Theory and applications of free-electron vortex states, *Physics Reports* **690**, 1 (2017).

[30] A. Plumadore and A. L. Harris, Projectile transverse momentum controls emission in electron vortex ionization collisions, *Journal of Physics B: Atomic, Molecular and Optical Physics* **53**, 205205 (2020).

[31] Analyst **141**, 4044 (2016).

[32] A. Zinoviev and K. Nordlund, Nuclear Instruments and Methods in Physics Research Section B: Beam Interactions with Materials and Atoms **406**, 511 (2017).

[33] Z. Bouchal and M. Olivík, Non-diffractive vector bessel beams, *Journal of Modern Optics* **42**, 1555 (1995).

[34] J. F. Rico, R. López, I. Ema, and G. Ramirez, Analysis of the molecular density: Sto densities, *The Journal of chemical physics* **117**, 533 (2002).

[35] J. Wright\*, C. Rowley, and L. Chepelev, A ‘universal’b3lyp-based method for gas-phase molecular properties: bond dissociation enthalpy, ionization potential, electron and proton affinity and gas-phase acidity, *Molecular Physics* **103**, 815 (2005).